crystals

MDPI

Article

Synthesis of Manganese Mononitride with Tetragonal Structure under Pressure

Dajian Huang [1], Caoping Niu [2,3], Bingmin Yan [1], Bo Gao [1], Lailei Wu [4], Dongzhou Zhang [5], Xianlong Wang [2,3,*] and Huiyang Gou [1,*]

1 Center for High Pressure Science and Technology Advanced Research, Beijing 100190, China; dajian.huang@hpstar.ac.cn (D.H.); bingmin.yan@hpstar.ac.cn (B.Y.); bo.gao@hpstar.ac.cn (B.G.)
2 Key Laboratory of Materials Physics, Institute of Solid State Physics, Chinese Academy of Sciences, Hefei 230031, China; cpniu@theory.issp.ac.cn
3 University of Science and Technology of China, Hefei 230026, China
4 State Key Laboratory of Metastable Materials Science and Technology, Yanshan University, Qinhuangdao 066004, China; wll@ysu.edu.cn
5 Hawai'i Institute of Geophysics and Planetology, School of Ocean and Earth Science and Technology, University of Hawai'i at Manoa, Honolulu, HI 96822, USA; dzhang@hawaii.edu
* Correspondence: xlwang@theory.issp.ac.cn (X.W.); huiyang.gou@hpstar.ac.cn (H.G.)

Received: 14 August 2019; Accepted: 27 September 2019; Published: 30 September 2019

Abstract: The exploration of the vast phase space of transition metal nitrides is critical for discovering novel materials and potential technological applications. Manganese mononitride with a tetragonal structure (space group *I*4/*mmm*) was synthesized in a laser-heating diamond anvil cell, which could be quenched to ambient pressure. The bulk modulus of 173 GPa was measured using in situ high-pressure diffraction, and the axial compressibility shows that, under pressure, the *a* direction is much more compressible than the *c* direction in tetragonal MnN. DFT results with correction of the on-site repulsion (GGA + *U*) confirm that tetragonal MnN is energetically stable and antiferromagnetic. This study highlights the need to include on-site repulsion to understand 3*d* metal nitrides.

Keywords: transition metal nitrides; MnN; high pressure laser heating; density functional theory

1. Introduction

Nitrogen is an abundant element in atmospheric conditions, and it can form a large number of important materials with main group elements and transition metal elements. Transition metal nitrides attract considerable interest due to their mechanical, electronic, and magnetic properties. For example, transition metal nitrides are considered to be potentially superhard materials [1] because of the strong hybridization between nitrogen and transition metals, giving them high incompressibility and hardness. Furthermore, the partially filled *d* orbitals of transition metals bonded with nitrogen also lead to the presence of interesting electronic and magnetic properties, which are also great candidates for magnetic storage devices [2].

At ambient pressure, most transition metal nitrides are prepared through traditional synthesis routes, such as ammonolysis or nitridation of metals and their compounds [3,4], vapor deposition [5], and epitaxial growth methods [6]. However, some binary nitrides are difficult to synthesize using standard methods, so high-pressure synthesis provides an alternative route for discovering novel nitrides. Recently, several novel transition metal nitrides have been synthesized in the Fe–N [7], Cu–N [8], Hf–N [9], and Ta–N [10] systems, suggesting that pressure can effectively promote the role of *d*-electrons in chemical bonding with nitrogen [11].

Manganese nitrides are particularly interesting because of their variety of electronic and magnetic properties. Experimentally, the perovskite-type ε-Mn_4N films showed ferromagnetic properties with a

magnetic moment of 1.1 μ_B per unit cell, and the tetragonal η-Mn_3N_2 films exhibited antiferromagnetism with 0.4 μ_B per unit cell [12]. So far, among the manganese nitrides, the most nitrogen rich-nitride is reported to be mononitride, θ-MnN (Space group:139), which has been synthesized using different methods, such as molecular beam epitaxy [13] and DC reactive sputtering [14]. Tetragonal MnN was found to have anomalous thermal expansion and be antiferromagnetic with a Néel temperature of 650 K [15]. Moreover, experimental data found that the magnetic structure of MnN consisted of ferromagnetically aligned *c*-planes coupled anti-ferromagnetically in the *c*-direction [16]. Here, we report the synthesis of the MnN compound starting from elemental Mn and liquid nitrogen in a laser-heated diamond anvil cell to explore the phase space of the Mn–N system. Tetragonal MnN was synthesized at 30 GPa and 1500 °C and was quenchable to ambient pressure. The bulk modulus and the axial compressibility were measured using in situ high-pressure diffraction. DFT results with GGA + *U* confirm that tetragonal MnN is energetically stable and antiferromagnetic.

2. Materials and Methods

Experimental details: A micrometer-sized manganese (99.95% Alfa Aesar) flake was placed into the gasket hole of a diamond anvil cell (DAC) and subsequently loaded with high-purity liquid nitrogen. Liquid nitrogen served both as a pressure medium and a reactant. A stainless-steel gasket was used to form the sample chamber in the experimental runs with 300 μm culets. The pressure was calibrated by the ruby fluorescence. After cold compression to a maximum pressure of 30.0 GPa, the sample was heated at about 1500 °C for about 5 min. The heating was performed using two 100 W YLF (yttrium lithium fluoride) fiber lasers within a double-sided infrared laser heating system at 16-IDB, High-Pressure Collaborative Access Team (HPCAT). Temperatures from both sides were measured individually with an imaging spectrograph [17]. Angle-dispersive powder X-ray diffraction patterns were collected before and after laser heating at HPCAT, beamline 16-IDB (wavelength: λ = 0.4066 Å) and GeoSoilEnviroCARS, beamline 13-BM-C (Wavelength: λ = 0.434 Å) of the Advanced Photon Source (APS), Argonne National Laboratory (ANL). The diffraction images were integrated using DIOPTAS [18], and Rietveld refinement with GSAS software was performed to obtain the unit cell volume and lattice parameters [19,20].

Computational details: Theoretical calculations were carried out using the Vienna ab initio approximation package (VASP) [21,22] within the generalized gradient approximation (GGA) parametrized by the Perdew–Burke–Ernzerhof (PBE) functional [23]. All structures were fully relaxed without symmetry constraints with a cutoff energy of 850 eV, and the convergence of energy and force were set to 1×10^{-6} eV and 0.001 eV/Å, respectively. The *k*-points were automatically generated by the Monkhorst–Pack grids with a resolution of 0.03 $Å^{-1}$ [24]. The projector-augmented plane-wave (PAW) potentials [24,25] were used. To accurately describe the strongly correlated interaction between MnN, FeN, and CrN, GGA + *U* was also employed to study the stability and electronic properties with a fixed *U* value of 4 eV. The phonon dispersion curves were calculated using the PHONOPY code with density-functional perturbation theory (DFPT) [26].

3. Results and Discussion

Elemental manganese and liquid nitrogen were loaded into a diamond anvil cell and compressed up to 30 GPa to obtain potential manganese nitrides. Before heating, we did not observe the formation of any new phases monitored with in situ synchrotron X-ray diffraction, except Mn and nitrogen (Figure 1a). Upon heating to 1500 °C, a new phase clearly is present in the observed diffraction pattern (Figure 1b), and heating was maintained for 5 min to complete the grain growth. The reaction was further reproduced by heating two or three different spots in the samples. At room temperature after heating, the powder X-ray diffraction patterns were collected from 30 GPa down to ambient pressure shown in Figure 1c. With decompression to zero pressure, the diffraction peaks maintain sharp and strong, suggesting the samples' stability and recovery at ambient pressure. The X-ray diffraction lines of MnN as a function of pressure are shown in Figure 2a. The smooth evolutions of the X-ray diffraction

lines reveal no phase transition in MnN during its recovery down to ambient conditions. The powder diffraction data for MnN at different pressures could be Rietveld refined with the space group of *I4/mmm* as plotted in Figure 2b,c. The crystal structure of MnN is given in Figure 2d, showing that each Mn atom has six nearest neighbors forming an octahedron. The lattice constants of the primitive tetragonal cell were a = 2.994(1) Å and c = 4.175(1) Å at zero pressure. The Mn and N atoms were located in the 2*a* (0, 0, 0) and 2*b* (0, 0, 0.5) Wyckoff positions. In a previous paper by Suzuki et al. [14], the cell was given as an F-cell with a = 4.256 Å and c = 4.189 Å, which transformed to primitive cell: a = 3.009 Å and c = 4.189 Å. Thus, our lattice constants are slightly smaller than those obtained by Suzuki et al. [14].

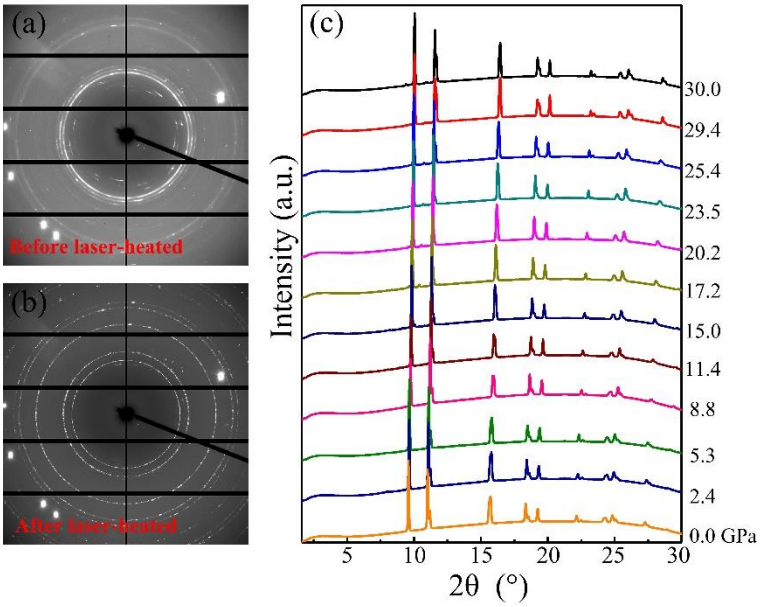

Figure 1. X-ray diffraction pattern of Mn and liquid N before (**a**) and after (**b**) laser heating at 30.0 GPa; (**c**) powder X-ray diffraction patterns of MnN from 30 GPa to ambient pressure.

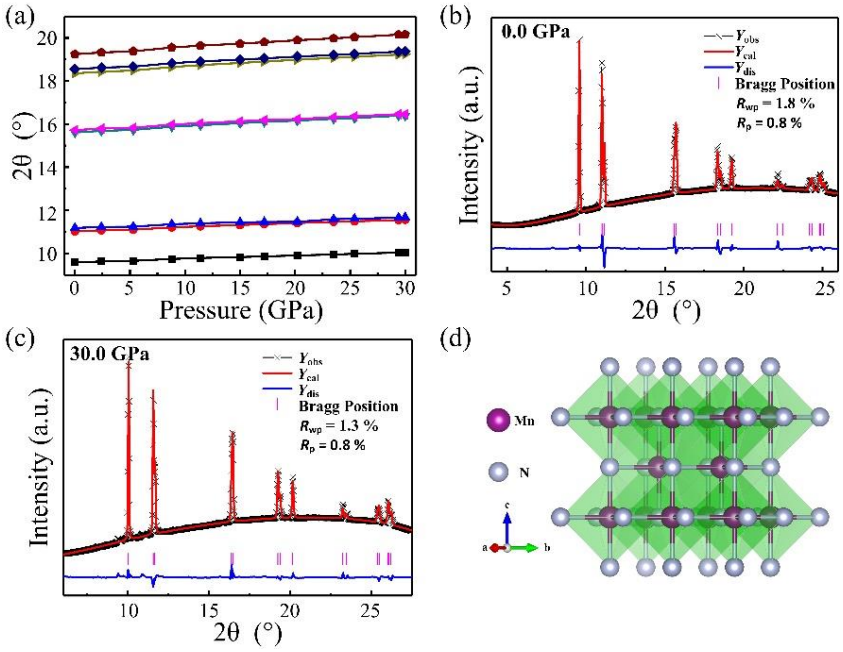

Figure 2. (**a**) X-ray diffraction lines' evolution with pressure; (**b**) crystal structure of MnN; Rietveld refinement of the XRD pattern of the MnN sample at (**c**) 0.0 GPa and (**d**) 30.0 GPa, respectively.

For comparison, the structural properties of the adjacent 3*d* transition metal nitrides (CrN and FeN) are listed in Table 1. Experimentally, the majority of rocksalt nitride compounds generally possess a relatively bigger bulk modulus than those of their corresponding pure metal elements, due to the hybridized *p*-*d* bonding of the transition metal and nitrogen. The pressure dependence of the unit cell volume and the lattice parameters are displayed in Figure 3a,b, respectively. The volume–pressure data were fitted with a third-order Birch–Murnaghan equation of state (EoS) to calculate both the zero-pressure bulk modulus, B_0, and its derivative with respect to pressure, B_0'. Three cases are discussed. Firstly, the resulting value is B_0 = 160 GPa if B_0' is fixed to the canonical value of 4. Secondly, the resulting value is B_0 = 191 GPa (with B_0' = 2.20) when V_0 is fixed to the value of 37.43 Å^3. Thirdly, if B_0' is allowed to freely vary, the resulting bulk modulus is 173 GPa and its derivative is 3.06. This means the data can be fitted almost equally well by decreasing the value of B_0 and increasing the value of B_0' or vice versa. The calculated bulk modulus is 187 GPa, in good agreement with the experimental value. Generally, for 3*d* transition metal nitrides with a rocksalt structure, the metals from Cr to Fe have a significantly decreasing bulk modulus with the increase of valence electrons. In addition, as shown in Figure 3b, as pressure increased, the lattice parameters show slightly anisotropic. The axial compressibility of lattice parameters shows that the decreasing of a/a_0 is larger than that of c/c_0 with increasing pressure, which means the material is much more compressible along the *a* direction than the *c* direction. At the pressure of 30 GPa, the *a* axis and *c* axis decrease by 4.59% and 4.16% relative to the ambient pressure value, respectively.

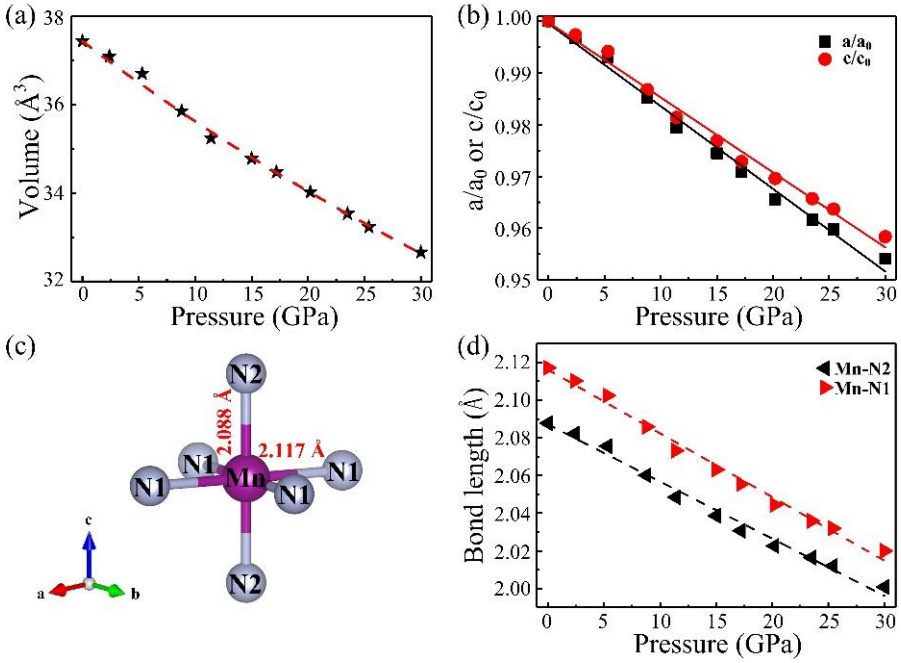

Figure 3. The changes of (**a**) unit cell volume and (**b**) lattice parameters in the entire pressure change; (**c**) The atomic arrangement of the MnN_6 octahedron; (**d**) Bond length of Mn–N as a function of pressure.

Pressure can effectively promote a chemical interaction between transition metal *d*-electrons and nitrogen, inevitably leading to interesting properties in these compounds. As plotted in Figure 3c, this atomic arrangement of MnN_6 octahedrons has a slight distortion and rotation at ambient pressure. To quantitatively illustrate the pressure-induced evolution of the Mn–N bonds in octahedron MnN_6, we further derived the Mn–N bond lengths from the Rietveld refinements, as depicted in Figure 3d. In the range of 0–30 GPa, the in-plane Mn–N1 bond length and the out-of-plane Mn–N2 bond length decrease gradually as pressure increases. The Mn–N1 and Mn–N2 bond lengths are 2.117 and 2.088 Å at zero pressure, respectively. The fitting curve shows that the descent rate of the Mn–N1 bond length

is larger than the Mn–N2, which corresponds to the decrease rate of a/a_0 larger than that of c/c_0, which results in much more compressibility along the *a* direction than along the *c* direction.

Table 1. Summary of crystal data of tetragonal MnN, and adjacent 3*d* transition metal nitrides. B_0 is the bulk modulus and $B_0^{'}$ its pressure derivative.

Compound	Space Group	Structure	Lattice Parameters (Å)	B_0 (GPa)	$B_0^{'}$	Ref.
CrN	*Fm*3*m*	RS		DFT: 340-430		[27]
CrN	*Pnma*	Orthorhombic		243(10)		[27]
MnN	*I*4/*mmm*	RS	a = 2.994(1) c = 4.175(1)	173 DFT: 187	3.06	Present
FeN	$Fm\bar{3}m$	RS	a = 4.1041	186	4.77	[28]
FeN	$F\bar{4}3m$	ZB	a = 4.2250	266	6.65	[28]

* RS represents rock-salt structure; ZB represents zinc blende structure.

To help to understand the origin of the stability and magnetic configurations of MnN, we calculated five possible candidates for MnN, including previously reported *I*4/*mmm*–MnN, $F\bar{4}3m$–MnN, $Fm\bar{3}m$–MnN, and the neighboring CrN- and FeN-type structures, *Pmmn*–MnN and $P6_3/mmc$–MnN. At first, we looked for the most stable magnetic ground states of MnN with different candidates at ambient conditions and considered three possible magnetic configurations (non-magnetic, ferromagnetic, and antiferromagnetic) in our calculations. Our results found that the antiferromagnetic state with a magnetic moment of 4.04 μ_B is the most stable magnetic configuration for all the candidates of MnN. Therefore, we only focused on the evolution of antiferromagnetic MnN structures with increasing pressure. The calculated enthalpies based on the GGA functional are plotted in Figure 4a, showing that $F\bar{4}3m$–MnN is the most stable at zero pressure. However, $P6_3/mmc$–MnN is the most stable crystal structure at high pressures ranging from 10 GPa to 100 GPa. Furthermore, to sufficiently describe the strongly correlated system of Mn–N, we also calculated the enthalpies of MnN structures by including the *U* correction, and the results are shown in Figure 4b. We found that the *I*4/*mmm*–MnN observed experimentally is the most stable at ambient conditions and remains stable at high pressure up to 75 GPa. The Pmmn–MnN had smaller enthalpy than *I*4/mmm–MnN at 80 GPa. Later, *I*4/*mmm*–MnN becomes the most stable structure again when the pressure increases to 100 GPa. These results indicate that correcting the strongly correlated interaction is very important for a precise understanding of MnN properties. Furthermore, based on the GGA+*U* method, the phonon dispersion curves of *I*4/*mmm*–MnN were calculated, as shown in Supplementary Materials Figure S1. The results indicate that imaginary frequency is not observed, revealing the dynamical stability of *I*4/*mmm*–MnN again at ambient conditions.

To provide a deeper understanding of the electronic properties of *I*4/*mmm*–MnN, the calculated band, and partial density of states (PDOS) were examined, as shown in Figure 5a. We can see that *I*4/*mmm*–MnN is metallic with electronic bands crossing the Fermi level (E_F). Assisted by the calculated density of states (DOS), we show that the conduction bands comprise of mixed Mn-*d* and N-*p* states. As we know that the magnetic ground state of *I*4/*mmm*-MnN is antiferromagnetic, the total DOS of the spin-up channel equals to that of spin-down channel. Furthermore, strong hybridization between the Mn–*d* orbitals and N–*p* orbitals is found, and both Mn–*d* orbitals and N–*p* orbitals mainly contribute to the states around the Fermi level. While formally metallic, the DOS at the Fermi energy is low (0.67 states/eV/cell). To compare the electronic properties of *I*4/*mmm*–MnN, we further investigated the stable configuration and electronic properties of FeN and CrN at zero pressure. Our results show that at ambient conditions, the most stable configuration of FeN and CrN is $F\bar{4}3m$- and $Fm\bar{3}m$-type structures, respectively. The magnetic ground state of both $F\bar{4}3m$–FeN and $Fm\bar{3}m$–CrN are antiferromagnetic with a magnetic moment of 3.85 μ_B and 2.49 μ_B, respectively. The band structures and PDOS are shown in Figure 5b,c. Both *I*4/*mmm*–MnN and $Fm\bar{3}m$–CrN are similar, showing metallic behaviors. However, the $F\bar{4}3m$–FeN is a semiconductor with a direct band gap of 0.5 eV at the *X* point.

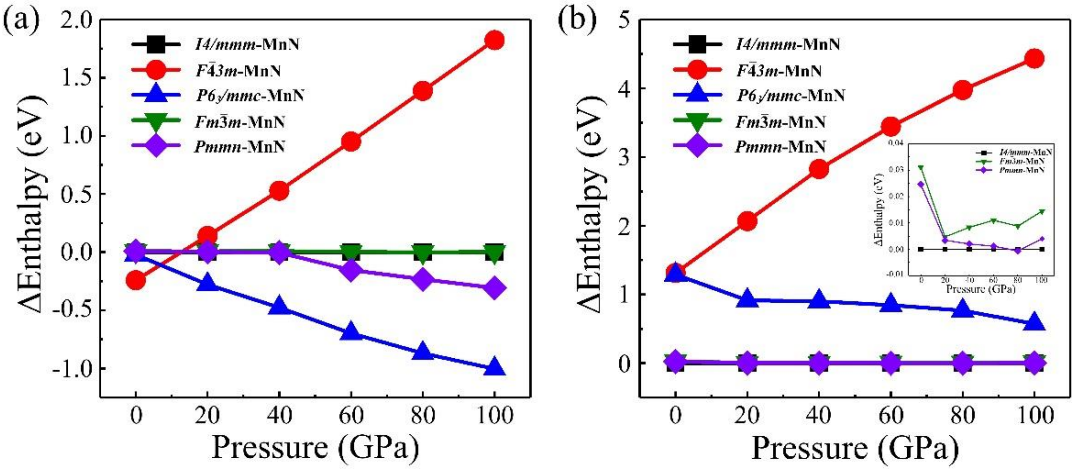

Figure 4. Enthalpies of MnN are shown as a function of pressure based on the DFT method (**a**) and DFT+*U* method (**b**). The enthalpy of MnN in phase A is set to zero, and contrasts between enthalpies of different phases are shown more clearly in the insets of (**b**).

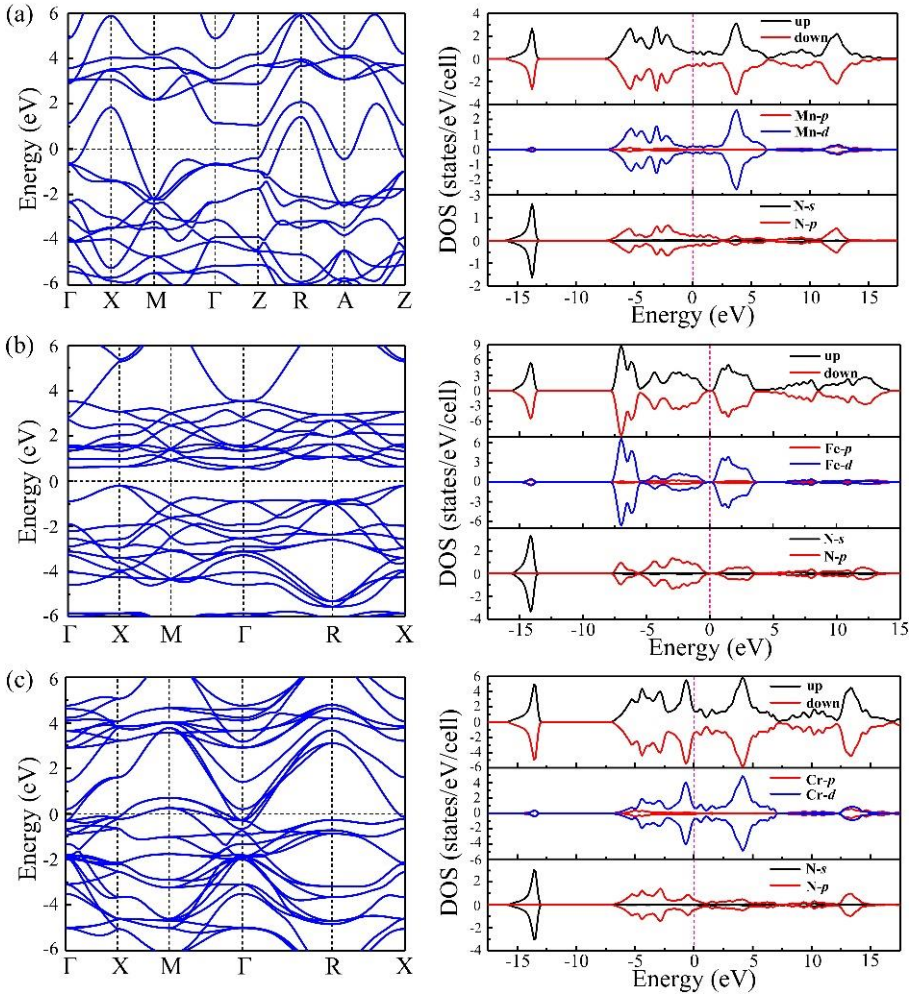

Figure 5. (**a**–**c**) show the band structures and density of states (DOS) of *I*4/*mmm*–MnN, *F*$\bar{4}$3*m*–FeN, and *Fm*$\bar{3}$*m*–CrN at zero pressure, respectively. The dashed lines show the Fermi level. For the density of states, the top, middle, and bottom part represent the total DOS, partial DOS of transitional metal elements, and partial DOS of N, respectively.

4. Conclusions

In this work, manganese and nitrogen were compressed and laser-heated at 30.0 GPa for the first time, which overcomes the energy barrier towards the formation of a more stable MnN compound. We performed Rietveld refinement to determine the structure of MnN, which is indexed by face-center tetragonal structure (space group *I*4/*mmm*). The compound is stable after quenching upon pressure release. Analysis of the lattice parameters and bond lengths found that the MnN is much more compressible along the *a* direction than along the *c* direction. In addition, the MnN volume–pressure data were fitted with an EoS to obtain the bulk modulus. Tetragonal MnN possesses a larger bulk modulus than the corresponding pure manganese elements due to the presence of hybridized *p*–*d* bonding. The theoretical calculations with on-site repulsion based on DFT support that MnN with an antiferromagnetic structure is the most stable structure from ambient to 75 GPa.

Supplementary Materials: The following are available online at http://www.mdpi.com/2073-4352/9/10/511/s1, Figure S1: The phonon dispersions of *I*4/*mmm*-MnN at 0 GPa.

Author Contributions: Conceptualization, H.G.; Formal analysis, D.H., C.N., L.W. and X.W.; Investigation, D.H., B.Y., B.G. and D.Z.; Supervision, H.G.; Writing – original draft, D.H. and C.N.; Writing – review & editing, X.W. and H.G.

Funding: This research was funded by the National Natural Science Foundation of China, grant number 11674329, and Science Challenge Project, grant number TZ2016001.

Acknowledgments: The laser-heating and in situ synchrotron XRD experiments were performed at 16IDB of HPCAT (Sector 16), and 13 IDD of GSECARS (Sector 13), Advanced Photon Source (APS), Argonne National Laboratory (ANL). HPCAT operations are supported by DOE-NNSA's Office of Experimental Sciences. GeoSoilEnviroCARS is supported by the National Science Foundation - Earth Sciences (EAR-1634415) and Department of Energy-GeoSciences (DE-FG02-94ER14466). Use of the COMPRES-GSECARS gas loading system was also supported by COMPRES under NSF Cooperative Agreement EAR -1606856. APS is a U.S. Department of Energy (DOE) Office of Science User Facility operated for the DOE Office of Science by ANL under Contract No. DE-AC02-06CH11357. The authors express great thanks to Freyja O'Toole for English editing.

Conflicts of Interest: The authors declare no conflict of interest.

References

1. Kaner, R.B.; Gilman, J.J.; Tolbert, S.H. Designing Superhard Materials. *Science* **2005**, *308*, 1268–1269. [CrossRef] [PubMed]
2. Coey, J.M.D.; Smith, P.A.I. Magnetic Nitrides. *J. Magn. Magn. Mater.* **1999**, *200*, 405–424. [CrossRef]
3. Oyama, S.T. *Chemistry of Transition Metal Carbides and Nitrides*; Springer: Berlin, Germany, 1996.
4. Herle, P.S.; Hegde, M.S.; Vasathacharya, N.Y.; Philip, S.; Rao, M.V.R.; Sripathi, T. Synthesis of TiN, VN, and CrN from Ammonolysis of TiS_2, VS_2, and Cr_2S_3. *J. Solid State Chem.* **1997**, *134*, 120–127. [CrossRef]
5. Kurtz, S.R.; Gordon, R.G. Chemical Vapor Deposition of Titanium Nitride at Low Temperatures. *Thin Solid Films* **1986**, *140*, 277–290. [CrossRef]
6. Zhang, X.Y.; Chawla, J.S.; Deng, R.P.; Gall, D. Epitaxial Suppression of the Metal-insulator Transition in CrN. *Phys. Rev. B* **2011**, *84*, 073101. [CrossRef]
7. Bykov, M.; Bykova, E.; Aprilis, G.; Glazyrin, K.; Koemets, E.; Chuvashova, I.; Kupenko, I.; McCammon, C.; Mezouar, M.; Prakapenka, V.; et al. Fe-N System at High Pressure Reveals a Compound Featuring Polymeric Nitrogen Chains. *Nat. Commun.* **2018**, *9*, 2756. [CrossRef]
8. Binns, J.; Donnelly, M.E.; Peña-Alvarez, M.; Wang, M.; Gregoryanz, E.; Hermann, A.; Dalladay-Simpson, P.; Howie, R.T. Direct Reaction between Copper and Nitrogen at High Pressures and Temperatures. *J. Phys. Chem. Lett.* **2019**, *10*, 1109–1114. [CrossRef]
9. Salamat, A.; Hector, A.L.; Gray, B.M.; Kimber, S.A.J.; Bouvier, P.; McMillan, P.F. Synthesis of Tetragonal and Orthorhombic Polymorphs of Hf_3N_4 by High-Pressure Annealing of a Prestructured Nanocrystalline Precursor. *J. Am. Chem. Soc.* **2013**, *135*, 9503–9511. [CrossRef]
10. Salamat, A.; Woodhead, K.; Shah, S.I.U.; Hector, A.L.; McMillan, P.F. Synthesis of U_3Se_5 and U_3Te_5 Type Polymorphs of Ta_3N_5 by Combining High Pressure–Temperature Pathways with a Chemical Precursor Approach. *Chem. Commun.* **2014**, *50*, 10041–10044. [CrossRef]

11. Utsumi, W.; Saitoh, H.; Kaneko, H.; Watanuki, T.; Aoki, K.; Shimomura, O. Congruent Melting of Gallium Nitride at 6 GPa and its Application to Single-Crystal Growth. *Nat. Mater.* **2003**, *2*, 735–738. [CrossRef]
12. Morio, K.; Koizumi, Y. Electronic Density of State of Mn-N Thin Films Measured by XPS. *J. Surf. Sci. Soc. Jpn.* **2003**, *24*, 480–484. [CrossRef]
13. Yang, H.; Al-Brithen, H.; Trifan, E.; Ingram, D.C.; Smith, A.R. Crystalline Phase and Orientation Control of Manganese Nitride Grown on MgO (001) by Molecular Beam Epitaxy. *J. Appl. Phys.* **2002**, *91*, 1053–1059. [CrossRef]
14. Suzuki, K.; Kaneko, T.; Yoshida, H.; Obi, Y.; Fujimori, H.; Morita, H. Crystal Structure and Magnetic Properties of the Compound MnN. *J. Alloys Compd.* **2000**, *306*, 66–71. [CrossRef]
15. Suzuki, K.; Suzuki, T.; Fujinaga, Y.; Kaneko, T.; Yoshida, H.; Obi, Y.; Tomiyoshi, S. A Nomalous Thermal Expansion of MnN. *J. Alloys Compd.* **2003**, *360*, 34–40. [CrossRef]
16. Suzuki, K.; Yamaguchi, Y.; Kaneko, T.; Yoshida, H.; Obi, Y.; Fujimori, H.; Morita, H. Neutron Diffraction Studies of the Compounds MnN and FeN. *J. Phys. Soc. Jpn.* **2001**, *70*, 1084–1089. [CrossRef]
17. Meng, Y.; Hrubiak, R.; Rod, E.; Boehler, R.; Shen, G.Y. New Developments in Laser-Heated Diamond Anvil Cell with *In-Situ* Synchrotron X-ray Diffraction at High Pressure Collaborative Access Team. *Rev. Sci. Instrum.* **2015**, *86*, 072201. [CrossRef] [PubMed]
18. Prescher, C.; Prakapenka, V.B. DIOPTAS: A Program for Reduction of Two-Dimensional X-ray Diffraction Data and Data Exploration. *High Pressure Res.* **2015**, *35*, 223–230. [CrossRef]
19. Larson, A.C.; Von Dreele, R.B. *General Structure Analysis System (GSAS)*; 2004. Available online: https://11bm.xray.aps.anl.gov/documents/GSASManual.pdf (accessed on 30 September 2019).
20. Toby, B.H. EXPGUI, a Graphical User Interface for GSAS. *J. Appl. Cryst.* **2001**, *34*, 210–213. [CrossRef]
21. Kresse, G.; Hafner, J. *Ab Initio* Molecular Dynamics for Open-Shell Transition Metals. *Phys. Rev. B* **1993**, *48*, 13115–13118. [CrossRef]
22. Kresse, G.; Furthmüller, J. Efficient Iterative Schemes for *Ab Initio* Total-Energy Calculations Using a Plane-wave Basis Set. *Phys. Rev. B* **1996**, *54*, 11169–11186. [CrossRef] [PubMed]
23. Perdew, J.P.; Burke, K.; Ernzerhof, M. Generalized Gradient Approximation Made Simple. *Phys. Rev. Lett.* **1996**, *77*, 3865–3868. [CrossRef] [PubMed]
24. Blöchl, P.E. Projector Augmented-Wave Method. *Phys. Rev. B* **1994**, *50*, 17953–17979. [CrossRef] [PubMed]
25. Kresse, G.; Joubert, D. From Ultrasoft Pseudopotentials to the Projector Augmented-Wave Method. *Phys. Rev. B* **1999**, *59*, 1758–1775. [CrossRef]
26. Baroni, S.; de Gironcoli, S.; Corso, A.D.; Giannozzi, P. Phonons and Related Crystal Properties from Density-functional Perturbation Theory. *Rev. Mod. Phys.* **2001**, *73*, 515–562. [CrossRef]
27. Rivadulla, F.; Bañobre-López, M.; Quintela, C.X.; Piñeiro, A.; Pardo, V.; Baldomir, D.; López-Quintela, M.A.; Rivas, J.; Ramos, C.A.; Salva, H.; et al. Reduction of the Bulk Modulus at High Pressure in CrN. *Nat. Mater.* **2009**, *8*, 947–951. [CrossRef] [PubMed]
28. Soni, H.R.; Mankad, V.; Gupta, S.K.; Jha, P.K. A First Principles Calculations of Structural, Electronic, Magnetic and Dynamical Properties of Mononitrides FeN and CoN. *J. Alloys Compd.* **2012**, *522*, 106–113. [CrossRef]